


## Observation of Attosecond Time Delays in Above-Threshold Ionization

Wenhai Xie<sup>✉</sup>, Zichen Li, Min Li<sup>✉</sup>,\* Yupeng Liu, Yang Liu, Chuanpeng Cao, Keyu Guo,  
Kunlong Liu<sup>✉</sup>, Yueming Zhou, and Peixiang Lu<sup>†</sup>

*Wuhan National Laboratory for Optoelectronics and School of Physics, Huazhong University of Science and Technology, Wuhan 430074, China*

 (Received 16 October 2023; revised 3 June 2024; accepted 2 October 2024; published 29 October 2024)

Attosecond-scale temporal characterization of photoionization is essential in understanding how light and matter interact on the most fundamental level. However, characterizing the temporal property of strong-field above-threshold ionization has remained unreached. Here, we propose a novel photoelectron interferometric method to disentangle the contribution of Coulomb effect from an attoclock, allowing us to clock energy-resolved time delays of strong-field above-threshold ionization. We disentangle two types of Coulomb effects for the attoclock, i.e., one arising from the Coulomb disturbance of a single electron trajectory and the second effect arising from the photoelectron phase space distortion due to the Coulomb field. We find that the second Coulomb effect manifests itself as an energy-resolved attosecond time delay in the electron emission, which is relevant to the effect of nonadiabatic initial longitudinal momentum at the tunnel exit. Our study further indicates a sensitivity of the time delay to the temporal profile of the released electron wave packet within one half laser cycle. The temporal width of the released electron wave packet is found to increase with energy, which contradicts the common assumption in the adiabatic picture.

DOI: [10.1103/PhysRevLett.133.183201](https://doi.org/10.1103/PhysRevLett.133.183201)

Strong-field ionization of atoms and molecules triggers a variety of interesting ultrafast phenomena, such as the generation of attosecond light pulses [1,2], strong-field photoelectron holography [3,4], and laser-induced electron diffraction [5,6]. Those phenomena are usually interpreted in terms of electron trajectories starting to propagate from a specific ionization time. Thus the ionization time is a significant parameter to characterize the temporal property of strong-field ionization, providing the foundation for all attosecond spectroscopies based on strong-field ionization. The ionization time can also provide valuable insights into a fundamental question of whether a maximal ionization rate appears at the instant of maximal electric field strength.

Attoclock, also known as attosecond angular streaking, is a primary method to measure the ionization time in strong-field ionization [7–12]. In this method, an elliptically (near-circularly) polarized femtosecond laser pulse is used to map the ionization time of an electron to its emission angle in the photoelectron momentum distribution (PMD). Usually, an offset angle between the most probable emission direction with respect to the minor axis of the laser ellipse was measured. This offset angle has been used to study the delay between the ionization time of the peak of the PMD and the field peak instant [13–16]. However, it is challenging to accurately extract the ionization time from the measured

offset angle since the offset angle is strongly influenced by the Coulomb potential. Thus, disentangling the Coulomb effect from the measured offset angle is key to extracting the timing information from the attoclock measurement, which is a crucial step toward solving the enduring puzzle of whether the tunneling process needs a finite time. Previously, one disentangled the effect of the Coulomb disturbance of a single electron trajectory due to Coulomb momentum transfer on the offset angle, while the Coulomb effect on the entire electron wave packet was ignored [16–18]. From the experimental perspective, the offset angle was usually obtained from the peak of the photoelectron angular distribution (PAD) by integrating over the electron energy. The electrons with different energies might be influenced differently by the Coulomb potential, which would affect the extraction of the timing information from the attoclock measurement.

Most of previous attoclock measurements were performed in the strong-field tunneling ionization regime. Extending the attoclock measurements to the nonadiabatic strong-field ionization involves considerable challenges [19]. First, the action of the Coulomb potential on the electron becomes stronger and may vary more obviously with the electron energy, complicating the understanding of the attoclock measurements. More importantly, several above-threshold ionization (ATI) ring structures spaced by the photon energy emerge in the PMD, which are usually interpreted as a result of multiphoton absorption. Those ATI structures make it difficult to distinguish the

\*Contact author: [mli@hust.edu.cn](mailto:mli@hust.edu.cn)

†Contact author: [lupeixiang@hust.edu.cn](mailto:lupeixiang@hust.edu.cn)

peak of the PMD, which requires an energy-resolved study of the attoclock measurement. However, disentangling timing information from an energy-resolved attoclock experiment has so far remained unreached.

In this Letter, we propose and demonstrate a novel method to retrieve energy-resolved ionization time from the offset angle of the ATI in the nonadiabatic strong-field ionization. This method combines the attoclock principle and a photoelectron interferometry, which is an extension of the reconstruction of attosecond beating by interference of two-photon transitions (RABBIT) to the strong-field ATI regime [20]. Using this combined method, we disentangle two kinds of Coulomb effects, i.e., Coulomb disturbance of a single electron trajectory and Coulomb-induced momentum space distortion of the released wave packet, from the offset angle. We find that the Coulomb-induced momentum space distortion effect manifests itself as an attosecond time delay in the ATI and becomes important in the nonadiabatic tunneling regime due to the nonzero nonadiabatic longitudinal momentum at the tunnel exit.

The scheme of probing the time delay in ATI is shown in Fig. 1. We add a weak 800-nm corotating circularly polarized laser field to a strong 400-nm elliptically polarized laser field [Fig. 1(a)]. The synthesized laser field can be written as [atomic units (a.u.) are used unless otherwise specified]

$$\mathbf{E}(t) = [E_{400} \sin(2\omega t + \phi) + E_{800} \sin(\omega t)]\mathbf{e}_x + [\epsilon E_{400} \cos(2\omega t + \phi) + E_{800} \cos(\omega t)]\mathbf{e}_y, \quad (1)$$

where  $E_{400}$  and  $E_{800}$  are the electric field strengths of the 400-nm and 800-nm components, respectively.  $\omega$  is the frequency of the 800-nm laser field.  $\phi$  is the relative phase.  $\epsilon$  is the ellipticity of the 400-nm laser pulse, which is 0.8 in this study. The electric field along the  $x$  direction is shown in Fig. 1(b). For a specific ATI, the electron might be most probably released with a time delay  $\delta t$  relative to the 400-nm field peak. The electron trajectories released every half cycle of the synthesized two-color laser field will interfere, leading to an oscillation of the electron yield in the PMD [Fig. 1(c)]. Therefore, the yield oscillation shows a phase shift with respect to the Coulomb-free case, which can be used to quantify the magnitude of the Coulomb disturbance of a single electron trajectory. Applying this photoelectron interferometric method to the attoclock experiment allows us to separate the contribution of the Coulomb disturbance effect  $\delta\theta_c$  from the offset angle  $\delta\theta$ . Thus we can obtain the deflection angle induced by the time delay  $\delta\theta_t$  and further extract the time delay  $\delta t$ .

We implemented this scheme using a cold-target recoil ion momentum spectroscopy (COLTRIMS) setup [21,22]. The experimental details can be found in Supplemental Material [23]. Briefly, the laser pulse centered at 800 nm was split in a Mach-Zehnder interferometer into two laser beams. One of the laser beams was propagated through a 300- $\mu\text{m}$ -thick  $\beta$ -barium borate (BBO) crystal for second harmonic generation. After the BBO, the generated 400-nm laser pulse was changed to elliptical polarization with  $\epsilon = 0.8$ . The major axis of the laser ellipse is along the  $x$  direction and the minor axis along the  $y$  direction. The other laser beam was changed to circular polarization by a quarter wave plate. A phase-locking system was employed to finely control the relative phase  $\phi$  of the two-color pulse [29,30]. Those two beams were recombined and focused by an  $f = 75$ -mm silver concave mirror into an Ar gas jet. The three-dimensional momenta of the resulting photoelectrons were detected using the COLTRIMS. The intensity of the 400-nm and 800-nm laser components was  $\sim 9 \times 10^{13}$  W/cm<sup>2</sup> and  $\sim 2 \times 10^{11}$  W/cm<sup>2</sup>, respectively.

The measured PMDs in a single-color 400-nm laser field and in the synthesized two-color laser field at  $\phi = 0$  are shown in Figs. 2(a) and 2(b), respectively. The PMD in the single-color 400-nm laser field shows several ATI rings separated by the 400-nm photon energy. For each ATI ring, the most probable emission angle shows a clear offset angle  $\delta\theta$  with respect to the minor axis of the laser ellipse. The offset angle increases with energy, as shown in Fig. 2(d), which is consistent with a previous experiment on atomic hydrogen [19]. Adding the weak 800-nm laser field, sideband peaks appear in the momentum spectrum, at energies that correspond to the absorption or emission of a single 800-nm photon [Fig. 2(b)]. The yield of the

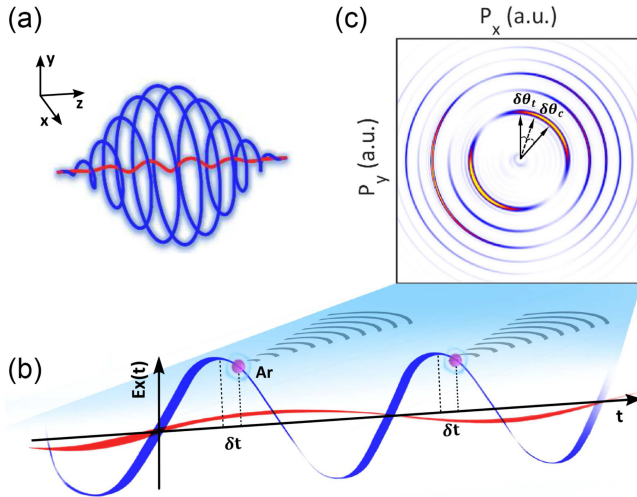


FIG. 1. The scheme of probing the time delay in ATI. (a) The synthesized two-color laser pulse consists of a strong 400-nm elliptically polarized field (blue) and a weak 800-nm circularly polarized field (red). (b) The 400- and 800-nm field components along the  $x$  direction. The electron for a specific ATI might be most probably released with a delay  $\delta t$  relative to the field peak of the 400-nm field. The released electron separated by every half cycle of the synthesized two-color laser field will interfere, leading to an oscillation of electron yield in the resulting PMD (c). The offset angle of an ATI ring  $\delta\theta$  is contributed by a deflection angle of  $\delta\theta_t$  and a deflection angle of  $\delta\theta_c$ . The PMD in (c) is obtained by numerically solving the time-dependent Schrödinger equation (TDSE) in the two-color laser field with  $\phi = 0$ .

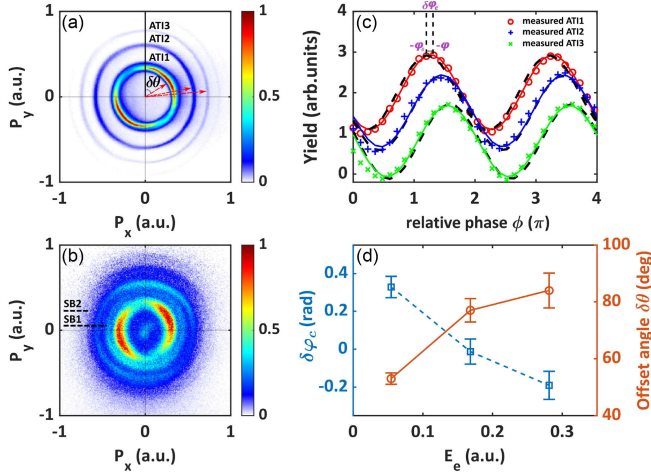


FIG. 2. (a) The measured PMD in a single-color 400-nm laser field. The most probable electron emission angles for the first three order ATIs are indicated by the red arrows. (b) The measured PMD in the two-color laser field at the relative phase of 0. (c) The yield of the first three order ATI as a function of the relative phase from the measurement. The yield are taken in the angular range from  $48^\circ$  to  $58^\circ$  for the first ATI, from  $72^\circ$  to  $82^\circ$  for the second ATI, and from  $79^\circ$  to  $89^\circ$  for the third ATI. The solid lines are the fitting results with cosine functions. For comparison, the Coulomb-free result, i.e.,  $\cos(\phi - \theta - \pi)$ , are shown by the dashed lines. The phase shift between the measurement and the Coulomb-free result is indicated by two vertical dashed lines. (d) The angular offset  $\delta\theta$  is plotted as a function of the electron energy from (a). For comparison, the phase shift  $\delta\varphi_c$  as a function of the electron energy is also shown.

electrons along the most probable emission direction for the first three ATIs as a function of the relative phase is shown in Fig. 2(c), which can be fitted using a function of  $Y = Y_0 + \Delta Y \cos(\phi + \varphi)$  with an oscillation phase of  $\varphi$ . In the Coulomb-free case, the oscillation phase can be expressed as  $\varphi_0 = -\theta - \pi$  [23], which only depends on the electron emission angle  $\theta = \arctan(p_y/p_x)$ , with  $p_x$  and  $p_y$  being the electron momenta along the major and minor axes of the elliptically polarized laser field, respectively. In Fig. 2(c), we also show the yield oscillation for the first three ATIs in the Coulomb-free case by the dashed line, i.e.,  $\cos(\phi - \theta - \pi)$ . A phase shift  $\delta\varphi_c = \varphi_0 - \varphi$  between the measurement and the Coulomb-free result can be seen. The phase shift  $\delta\varphi_c$  can be used to quantify the magnitude of the Coulomb disturbance of a single electron trajectory since the yield oscillation comes from the interference of several electron trajectories for a specific final momentum. As shown in Fig. 2(d), the phase shift  $\delta\varphi_c$  decreases with increasing the electron energy, meaning that the electron with larger energy experiences a smaller Coulomb disturbance interaction. This can be explained by the fact that the more energetic photoelectron spends less time interacting with the ionic core [31,32].

Surprisingly, comparing the phase shift  $\delta\varphi_c$  with the offset angle  $\delta\theta$  in Fig. 2(d), we find that they present

opposite trends with respect to the electron energy, i.e., the offset angle increases while the phase shift  $\delta\varphi_c$  decreases with increasing the electron energy. This indicates that the offset angle of the ATI is not purely contributed by the Coulomb disturbance of a single electron trajectory due to Coulomb momentum transfer. The opposite trend of those two observables provides an unambiguous evidence for the existence of a nonvanishing time delay between the ionization time of the ATI and the field peak in the elliptically polarized laser field.

To extract the time delay, we establish a relationship between the phase shift  $\delta\varphi_c$  and the angular shift in the PMD. We find that the phase shift  $\delta\varphi_c$  can be mapped onto a Coulomb-induced angular shift  $\delta\theta_c$  by the relation  $\delta\theta_c = \delta\varphi_c + \varphi_{clc}$  (see Supplemental Material for details [23]). Here  $\varphi_{clc}$  comes from the coupling between the Coulomb field and the weak 800-nm laser field, which is similar to the Coulomb-laser-coupling delay in the attosecond streaking [33–35]. In Fig. 3(a), we show the calculated  $\delta\theta_c$  as a function of the phase shift  $\delta\varphi_c$  for the first three ATI peaks using the Coulomb-corrected strong-field approximation (CCSFA) method [36–39]. The relation of  $\delta\theta_c = \delta\varphi_c + \varphi_{clc}$  is shown by the red solid line, which agrees with the simulated result. Then the ionization time delay is obtained using the attoclock principle [23],

$$\delta t = (\delta\theta - \delta\theta_c)/k_e. \quad (2)$$

Here  $k_e$  is the slope of the time-to-angle mapping relation according to the attoclock principle, which depends on the electron energy [11]. In Fig. 3(b), we show the extracted time delay as a function of the electron energy from the measurement and the TDSE simulation. The TDSE simulation agrees well with the measurement. The extracted time delay increases with the electron energy. For the first-order ATI, the electron is most probably released at near the

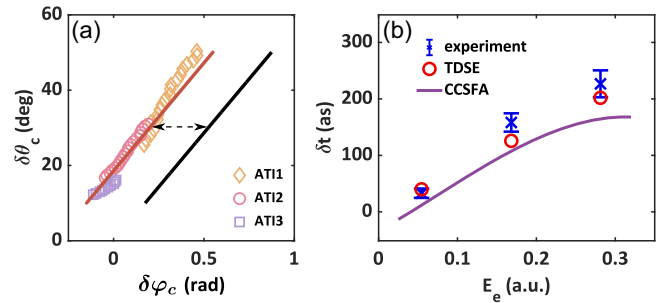


FIG. 3. (a) The calculated  $\delta\theta_c$  as a function of the phase shift  $\delta\varphi_c$  for the first three ATIs by the CCSFA simulation. The black solid line shows  $\delta\theta_c = \delta\varphi_c$ . The red solid line shows  $\delta\theta_c = \delta\varphi_c + \varphi_{clc}$ , where  $\varphi_{clc}$  is indicated by the dashed arrow. (b) The extracted ionization time delays from the measurement and TDSE as a function of the electron energy according to Eq. (2). The ionization time for the most probable electron trajectory of the ATI in a single-color 400-nm laser field calculated by the CCSFA simulation is shown by the solid line.

field maximum while the electron of the third-order ATI is most probably released with a time delay of almost 200 as relative to the field peak. Note that the time delay is different from the tunneling time [15,40].

To understand the mechanisms underlying the time delay, we obtain the ionization time of each ATI in a single-color 400-nm laser field by tracing the most probable electron trajectory back to the tunnel exit position using the CCSFA simulations. As shown by the solid line in Fig. 3(b), the ionization time of the most probable electron trajectory using the CCSFA qualitatively agrees with the extracted time delays from the measurement and TDSE simulation. A small discrepancy between the CCSFA and the measurement for the third ATI might come from the under-the-barrier Coulomb effect, which is ignored in the CCSFA method. We further show in Fig. 4(a) a series of electron trajectories released within one half cycle of the 400-nm elliptically polarized laser field. The electron-ion distance  $r$  for the electron released before the field maximum (red curves) continuously increases while that for the electron released after the field maximum (blue curves) decreases first and then increases over time. This means that the electron wave packet released within a half laser cycle is distorted in the momentum space. The electron released after the field peak instant experiences

a Coulomb scattering process at near the tunnel exit, which can be more clearly seen in Fig. 4(b) (solid lines). This Coulomb scattering originates from the fact that the electron released after the field maximum achieves a nonzero momentum pointing toward the ionic core at the tunnel exit, which is called initial longitudinal momentum [41,42]. Thus the electron initially moves toward the ionic core and experiences the Coulomb scattering. For the electron released before the field maximum, the direction of the initial longitudinal momentum is reversed [41,42], precluding the Coulomb scattering process. By setting the initial longitudinal momentum to be zero, the Coulomb scattering disappears, as shown by the dashed curves in Fig. 4(b). Due to the Coulomb scattering process, the electron wave packet is dramatically distorted, shifting the maximal ionization rate from the field peak instant to a later moment. The increasing time delay in Fig. 3(b) indicates that the high-energy electron is more easily distorted by the Coulomb potential, though it experiences a smaller Coulomb disturbance interaction.

To illustrate how the distortion effect leads to the time delay, we show in Fig. 4(c) the normalized PAD of the first three ATIs using the SFA, which suggests that the increasing width of the PAD (corresponding to the temporal width of the released wave packet) correlates with the increasing time delay. To verify this relation, we calculate the PAD by considering the Coulomb distortion effect using a simple method: the PAD calculated by the strong-field approximation (SFA) [Fig. 4(c)] is shifted by a deflection angle originating from the Coulomb-distortion effect [23]. As shown in Fig. 4(d), the peaks of the PADs appear at different angles for different ATIs. The most probable emission angle increases with the electron energy, indicating a larger time delay for higher order ATIs. Therefore, the extracted time delay can be used to characterize the temporal profile of the released wave packet in the elliptically polarized laser field. Our experiment shows that the temporal width of the released wave packet increases with energy. This does not concur with the assumption in the adiabatic picture, in which the temporal width of the released wave packet is independent on the electron energy [43].

In conclusion, we find an energy-dependent time delay between the ionization time of the ATI and the field peak instant in elliptically polarized laser pulses. Combining a RABBIT-like interferometric method with the attoclock principle, we have extracted this time delay with attosecond precision. We find that the time delay originates from the Coulomb-induced distortion effect, which is relevant to a Coulomb scattering process driven by the nonzero non-adiabatic longitudinal momentum at the tunnel exit. Our work highlights the importance of wave packet distortion due to the Coulomb field, which is ubiquitous, in strong-field ionization of atoms and molecules. For instance, the wave packet is strongly distorted by the Coulomb potential

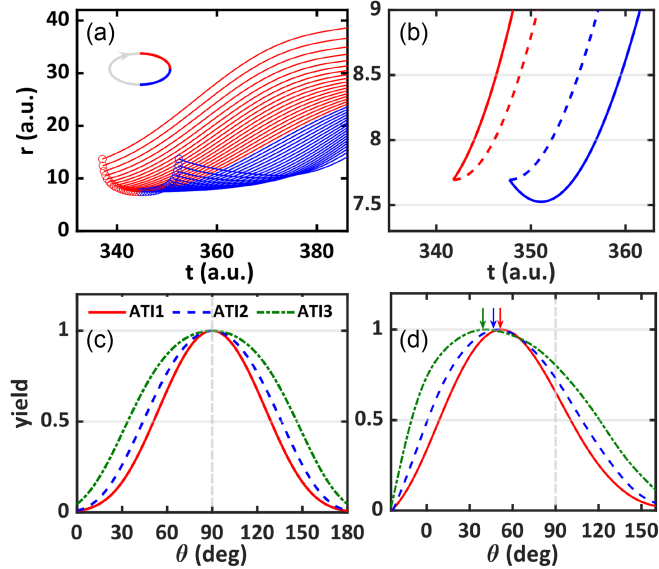


FIG. 4. (a) The electron trajectories released before (red) and after (blue) the field peak instant within a half cycle of a 400-nm elliptically polarized laser field. (b) The electron trajectories released at the instants of  $t_0 = t_p - 2.9$  a.u. (red solid line) and  $t_0 = t_p + 2.9$  a.u. (blue solid line) with  $t_p = 344.7$  a.u. being the field peak instant. The dashed lines show the corresponding electron trajectories by setting the initial longitudinal momentum to be zero. (c) The angular distribution for the first three ATIs calculated by the SFA model. (d) The same as (c) but considering the Coulomb distortion effect (see text for details). The arrows in (d) indicate the peaks of the angular distributions.

during the electron motion under the tunneling barrier. It will be intriguing to explore how the Coulomb-induced distortion affects the electron dynamics under the tunneling barrier. A possible approach is applying our scheme to oriented molecules, in which the Coulomb effect after the tunneling is nearly the same for different molecular orientations [44]. By comparing the results of different orientations, one can disentangle Coulomb-induced distortion effect during the quantum tunneling process. Our work also has a strong impact on the interpretation of the energy-resolved attoclock experiments, providing absolute timing information when clocking atomic-scale electron motion, e.g., time-resolved nondipole effect [45,46] and Auger-Meitner decay [12].

*Acknowledgments*—This work is supported by the National Key Research and Development Program of China (Grant No. 2023YFA1406800), the National Natural Science Foundation of China (Grants No. 62275085 and No. 12021004), and the Fundamental Research Funds for the Central Universities.

W. X. and Z. L. contributed equally to this letter.

- 
- [1] P. M. Paul, E. S. Toma, P. Breger, G. Mullot, F. Augé, Ph. Balcou, H. G. Muller, and P. Agostini, *Science* **292**, 1689 (2001).
- [2] M. Hentschel, R. Kienberger, Ch. Spielmann, G. A. Reider, N. Milosevic, T. Brabec, P. Corkum, U. Heinzmann, M. Drescher, and F. Krausz, *Nature (London)* **414**, 509 (2001).
- [3] Y. Huismans *et al.*, *Science* **331**, 61 (2011).
- [4] W. Xie, J. Yan, M. Li, C. Cao, K. Guo, Y. Zhou, and P. Lu, *Phys. Rev. Lett.* **127**, 263202 (2021).
- [5] M. Meckel *et al.*, *Science* **320**, 1478 (2008).
- [6] C. I. Blaga, J. Xu, A. D. DiChiara, E. Sistrunk, K. Zhang, P. Agostini, T. A. Miller, L. F. DiMauro, and C. D. Lin, *Nature (London)* **483**, 194 (2012).
- [7] P. Eckle, A. N. Pfeiffer, C. Cirelli, A. Staudte, R. Dörner, H. G. Muller, M. Büttiker, and U. Keller, *Science* **322**, 1525 (2008).
- [8] L. Torlina *et al.*, *Nat. Phys.* **11**, 503 (2015).
- [9] U. Sainadh, H. Xu, X. Wang, A. Atia-Tul-Noor, W. Wallace, N. Douguet, A. Bray, I. Ivanov, K. Bartschat, A. Kheifets, R. Sang, and I. Litvinyuk, *Nature (London)* **568**, 75 (2019).
- [10] A. N. Pfeiffer, C. Cirelli, M. Smolarski, D. Dimitrovski, M. Abu-samha, L. B. Madsen, and U. Keller, *Nat. Phys.* **8**, 76 (2012).
- [11] M. Han, P. Ge, J. Wang, Z. Guo, Y. Fang, X. Ma, X. Yu, Y. Deng, H. J. Wörner, Q. Gong, and Y. Liu, *Nat. Photonics* **15**, 765 (2021).
- [12] S. Li *et al.*, *Science* **375**, 285 (2022).
- [13] A. S. Landsman, M. Weger, J. Maurer, R. Boge, A. Ludwig, S. Heuser, C. Cirelli, L. Gallmann, and U. Keller, *Optica* **1**, 343 (2014).
- [14] N. Camus, E. Yakaboylu, L. Fechner, M. Klaiber, M. Laux, Y. Mi, K. Z. Hatsagortsyan, T. Pfeifer, C. H. Keitel, and R. Moshhammer, *Phys. Rev. Lett.* **119**, 023201 (2017).
- [15] H. Ni, U. Saalmann, and J. M. Rost, *Phys. Rev. Lett.* **117**, 023002 (2016).
- [16] M. Han, P. Ge, Y. Fang, X. Yu, Z. Guo, X. Ma, Y. Deng, Q. Gong, and Y. Liu, *Phys. Rev. Lett.* **123**, 073201 (2019).
- [17] A. W. Bray, S. Eckart, and A. S. Kheifets, *Phys. Rev. Lett.* **121**, 123201 (2018).
- [18] W. Quan, V. V. Serov, M. Wei, M. Zhao, Y. Zhou, Y. Wang, X. Lai, A. S. Kheifets, and X. Liu, *Phys. Rev. Lett.* **123**, 223204 (2019).
- [19] D. Trabert, N. Anders, S. Brennecke, M. S. Schöffler, T. Jahnke, L. P. H. Schmidt, M. Kunitski, M. Lein, R. Dörner, and S. Eckart, *Phys. Rev. Lett.* **127**, 273201 (2021).
- [20] L. J. Zipp, A. Natan, and P. H. Bucksbaum, *Optica* **1**, 361 (2014).
- [21] R. Dörner, V. Mergel, O. Jagutzki, L. Spielberger, J. Ullrich, R. Moshhammer, and H. Schmidt-Böcking, *Phys. Rep.* **330**, 95 (2000).
- [22] J. Ullrich, R. Moshhammer, A. Dorn, R. Dörner, L. Ph. H. Schmidt, and H. Schmidt-Böcking, *Rep. Prog. Phys.* **66**, 1463 (2003).
- [23] See Supplemental Material at <http://link.aps.org/supplemental/10.1103/PhysRevLett.133.183201> for details about the experiment and the extraction procedure of the ionization time delay, which includes Refs. [24–28].
- [24] Y. Feng, M. Li, S. Luo, K. Liu, B. Du, Y. Zhou, and P. Lu, *Phys. Rev. A* **100**, 063411 (2019).
- [25] W. Becker, F. Grasbon, R. Kopold, D. B. Milošević, G. G. Paulus, and H. Walther, *Adv. At. Mol. Opt. Phys.* **48**, 35 (2002).
- [26] D. B. Milošević, G. G. Paulus, D. Bauer, and W. Becker, *J. Phys. B* **39**, R203 (2006).
- [27] S. Skruszewicz, J. Tiggesbäumker, K.-H. Meiwes-Broer, M. Arbeiter, T. Fennel, and D. Bauer, *Phys. Rev. Lett.* **115**, 043001 (2015).
- [28] B. Hu, J. Liu, and S. G. Chen, *Phys. Lett. A* **236**, 533 (1997).
- [29] K. Lin *et al.*, *J. Phys. B* **49**, 025603 (2016).
- [30] X. Gong, C. Lin, F. He, Q. Song, K. Lin, Q. Ji, W. Zhang, J. Ma, P. Lu, Y. Liu, H. Zeng, W. Yang, and J. Wu, *Phys. Rev. Lett.* **118**, 143203 (2017).
- [31] K. Liu, S. Luo, M. Li, Y. Li, Y. Feng, B. Du, Y. Zhou, P. Lu, and I. Barth, *Phys. Rev. Lett.* **122**, 053202 (2019).
- [32] E. Bloch *et al.*, *Phys. Rev. X* **11**, 041056 (2021).
- [33] C.-H. Zhang and U. Thumm, *Phys. Rev. A* **82**, 043405 (2010).
- [34] S. Nagele, R. Pazourek, J. Feist, K. Doblhoff-Dier, C. Lemell, K. Tórkési, and J. Burgdörfer, *J. Phys. B* **44**, 081001 (2011).
- [35] M. Ivanov and O. Smirnova, *Phys. Rev. Lett.* **107**, 213605 (2011).
- [36] S. V. Popruzhenko and D. Bauer, *J. Mod. Opt.* **55**, 2573 (2008).
- [37] S. V. Popruzhenko, G. G. Paulus, and D. Bauer, *Phys. Rev. A* **77**, 053409 (2008).
- [38] T. M. Yan, S. V. Popruzhenko, M. J. J. Vrakking, and D. Bauer, *Phys. Rev. Lett.* **105**, 253002 (2010).
- [39] S. Brennecke, N. Eicke, and M. Lein, *Phys. Rev. Lett.* **124**, 153202 (2020).
- [40] M. Klaiber, Q. Z. Lv, S. Sukiasyan, D. Bakucz Canário, K. Z. Hatsagortsyan, and C. H. Keitel, *Phys. Rev. Lett.* **129**, 203201 (2022).

- [41] M. Li, H. Xie, W. Cao, S. Luo, J. Tan, Y. Feng, B. Du, W. Zhang, Y. Li, Q. Zhang, P. Lan, Y. Zhou, and P. Lu, *Phys. Rev. Lett.* **122**, 183202 (2019).
- [42] A. Geyer, D. Trabert, M. Hofmann, N. Anders, M. S. Schöffler, L. Ph. H. Schmidt, T. Jahnke, M. Kunitski, R. Dörner, and S. Eckart, *Phys. Rev. Res.* **5**, 033094 (2023).
- [43] M. V. Ammosov, N. B. Delone, and V. P. Krainov, *Sov. Phys. JETP* **64**, 1191 (1986).
- [44] J. Yan, W. Xie, M. Li, K. Liu, S. Luo, C. Cao, K. Guo, W. Cao, P. Lan, Q. Zhang, Y. Zhou, and P. Lu, *Phys. Rev. A* **102**, 013117 (2020).
- [45] B. Willenberg, J. Maurer, B. W. Mayer, and U. Keller, *Nat. Commun.* **10**, 5548 (2019).
- [46] H. Ni, S. Brennecke, X. Gao, P.-L. He, S. Donsa, I. Březinová, F. He, J. Wu, M. Lein, X.-M. Tong, and J. Burgdörfer, *Phys. Rev. Lett.* **125**, 073202 (2020).